Boundary slip from the immersed boundary lattice Boltzmann models

Guigao Le[1,*] and Junfeng Zhang[2,†]
[1]*School of Mechanical Engineering, Nanjing University of Science and Technology, Nanjing 210094, China*
[2]*School of Engineering, Laurentian University, 935 Ramsey Lake Road, Sudbury, ON, Canada P3E 2C6*
(Received 24 September 2008; published 5 February 2009)

We report an interesting and important observation of the velocity fields from immersed boundary lattice Boltzmann methods (IB-LBM). The computed velocity profiles can deviate from theoretical predictions greatly even for very simple flow situations, both in the immersed boundary layer and the bulk region. A rigorous analysis of the IB-LBM simulated velocity for a symmetric shear flow is carried out, and the analytical solutions indicate a strong dependence of velocity on the relaxation parameter (kinetic viscosity). Also our simulations demonstrate that simply increasing the immersed boundary layer thickness is not an efficient approach to reduce such velocity discrepancy. We hope this work will bring the awareness of this essential issue to people using IB-LBM for various flow situations.

DOI: 10.1103/PhysRevE.79.026701 PACS number(s): 47.11.−j, 83.50.Rp, 02.70.Ns

I. INTRODUCTION

In the 1970s, Peskin [1] developed the immersed boundary method (IBM) to simulate blood flows in hearts. The membrane-fluid interaction is accomplished by distributing membrane forces to the local fluid and by updating the membrane configuration according to local flow velocity. The attractiveness of such a treatment is that the fluid flow can be solved by appropriate numerical schemes over a fixed, regular Eulerian mesh, and therefore one can avoid the moving boundary problem. Since then, IBM has been widely used to study a variety of situations, including cell deformation in micropipettes [2], leukocyte adhesion and movement [3], multiphase flows [4], red blood cell deformation and aggregation [5,6], and the behavior of biofilms [7]. IBM has also been adopted to achieve a no-slip boundary of a moving solid surface [8,9]. Extensive reviews of the development and applications of IBM can be found elsewhere [10,11].

The lattice Boltzmann method (LBM) is a relatively newly developed simulation technique for complex fluid systems [12–14]. Originating form the classical statistical physics, LBM is a mesoscopic method, in which the fluid is modeled as a collection of pseudoparticles, and such particles propagate and collide over a discrete lattice domain. Macroscopic continuity and momentum equations can be obtained from this propagation-collision dynamics through a mathematical analysis [15]. The particulate nature and local dynamics provide advantages for complex boundaries and parallel computation. By incorporating the effects of microscopic interactions, multiphase fluids and surface wettability can also be simulated [16,17]. Successful LBM applications include multiphase flows in porous materials [18], solid-fluid interfacial phenomena [19,20], multiphase flows [21], non-Newtonian flows [18], droplet electrohydrodynamic deformation [22], and electrokinetics in microchannels [23].

Recently, these two numerical schemes have been integrated to exploit the synergy of IBM and LBM. Zhang *et al.* [24,25] investigated red blood cells in shear and channel flows, and several interesting microscopic hemodynamics characteristics have been observed, including the tank-treading motions, cell migration from the vessel wall, slipper-shaped cell deformation, cell-free layers, blunt velocity profiles and the Fahraeus effect. Here the membrane force was evaluated from the intercellular interaction and cell deformation through a physical constitute relationship. On the other hand, several immersed boundary lattice Boltzmann models (IB-LBM) have been proposed to simulated solid particles and moving boundaries in flows [26–29]. The difference among these models lies in the different approaches to calculate the required boundary force to enhance the no-slip boundary condition. For example, Feng *et al.* [26] assumed the solid particles are slightly deformable with a high stiffness and the boundary force was obtained as the spring force between a particle node and its imaginary reference one. Niu *et al.* [27] calculated the boundary force by the momentum exchange of the particle density distributions at boundary. In addition, Dupuis *et al.* [29] implemented a computational fluid mechanics IBM scheme [8], where the boundary force was obtained by comparing the desired boundary velocities to that computed without applying the boundary force. No master by which approaches of the boundary force is calculated, in all these IB-LBM models, this boundary force must be distributed to the fluid in a thin layer along the boundary.

Although careful efforts had been devoted to enhance the no-slip condition between the fluid and solid in these IB-LBM models, our recent simulations indicate that large boundary slip occurs and it may therefore destroy the simulation validity and usefulness. Several flow situations have been examined, including plainer and cylindrical Couette flows. The velocity profiles from IB-LBM simulations are compared to fluid mechanics and surprising deviations have been observed. For a better understanding of this interesting and important phenomenon, a rigorous analysis of the LBM velocity is conducted for the symmetric shear flow. Analytic relationships of the imposed boundary velocity, resulting LBM boundary velocity, boundary slip velocity, shear veloc-

*leguigao@mail.njust.edu.cn
FAX: (+8625) 8431–5831
†Fax: (705) 675-4862; jzhang@laurentian.ca

ity gradient, and boundary force have been derived, and they indeed are functions of both fluid and geometric parameters. These results show that a meaningful IB-LBM simulation should employ a small viscosity and/or a small lattice mesh size. Moreover, simulations demonstrate that simply increasing the immersed boundary layer (IBL) thickness cannot efficiently solve the boundary slip problem.

II. THEORY AND METHODS

A. Lattice Boltzmann method

In LBM, a fluid is modeled as pseudoparticles moving over a lattice domain at discrete time steps. The major variable in LBM is the density distribution $f_i(\mathbf{x},t)$, indicating the particle amount moving in the ith lattice direction at position $\mathbf{x}$ and time t. The time evolution of density distributions is governed by the so-called lattice Boltzmann equation, which is a discrete version of the Boltzmann equation in classical statistical physics [14,16],

$$f_i(\mathbf{x}+\mathbf{c}_i\delta_t,t+\delta_t)=f_i(\mathbf{x},t)+\Omega_i(f), \tag{1}$$

where $\mathbf{c}_i$ denotes the ith lattice velocity, δ_t is the time step, and Ω_i is the collision operator incorporating the change in f_i due to the particle collisions at a lattice node. The collision operator is typically simplified by the Bhatnagar-Gross-Krook (BGK) single-time-relaxation approximation [15],

$$\Omega_i(f)=-\frac{f_i(\mathbf{x},t)-f_i^{\mathrm{eq}}(\mathbf{x},t)}{\tau}, \tag{2}$$

where τ is a relaxation parameter and the equilibrium distribution f_i^{eq} can be expressed, for example, as [19]

$$f_0^{\mathrm{eq}}=\rho\left(1-\frac{2}{3c^2}\mathbf{u}^2\right),$$

$$f_i^{\mathrm{eq}}=\rho\left(\frac{1}{9}+\frac{1}{3c^2}\mathbf{c}_i\cdot\mathbf{u}+\frac{1}{2c^4}(\mathbf{c}_i\cdot\mathbf{u})^2-\frac{1}{6c^2}\mathbf{u}^2\right),\quad i=1-4,$$

$$f_i^{\mathrm{eq}}=\rho\left(\frac{1}{36}+\frac{1}{12c^2}\mathbf{c}_i\cdot\mathbf{u}+\frac{1}{8c^4}(\mathbf{c}_i\cdot\mathbf{u})^2-\frac{1}{24c^2}\mathbf{u}^2\right),\quad i=5-8, \tag{3}$$

for a D2Q9 (two dimensions, nine lattice velocities) lattice structure with lattice velocities $\mathbf{c}_i$,

$$\mathbf{c}_0=\mathbf{0},$$

$$\mathbf{c}_i=\left(\cos\frac{i-1}{2}\pi,\sin\frac{i-1}{2}\pi\right)c,\quad i=1-4,$$

$$\mathbf{c}_i=\sqrt{2}\left(\cos\frac{2i-9}{4}\pi,\sin\frac{2i-9}{4}\pi\right)c,\quad i=5-8, \tag{4}$$

where $c=\delta_x/\delta_y$, and δ_x is the lattice unit. Here $\rho=\Sigma_i f_i$ is the fluid density and $\mathbf{u}=\Sigma_i f_i\mathbf{c}_i/\rho$ is the fluid velocity. Through the Chapman-Enskog expansion, one can recover the macroscopic continuity and momentum (Navier-Stokes) equations from the above-defined LBM microdynamics,

$$\frac{\partial\rho}{\partial t}+\nabla(\rho\cdot\mathbf{u})=0,$$

$$\frac{\partial\mathbf{u}}{\partial t}+(\mathbf{u}\cdot\nabla)\mathbf{u}=-\frac{1}{\rho}\nabla p+\nu\nabla^2\mathbf{u}, \tag{5}$$

where p is the pressure and ν is the kinematic shear viscosity given by

$$\nu=\frac{2\tau-1}{6}\frac{\delta_x^2}{\delta_t}. \tag{6}$$

It can be seen from the above description that the microscopic LBM dynamics is local (i.e., only the very neighboring lattice nodes are involved to update the density distribution f_i), and hence a LBM algorithm is advantageous for parallel computations [14]. Also its particulate nature allows it to be relatively easily applied to systems with complex boundaries, such as flows in porous materials.

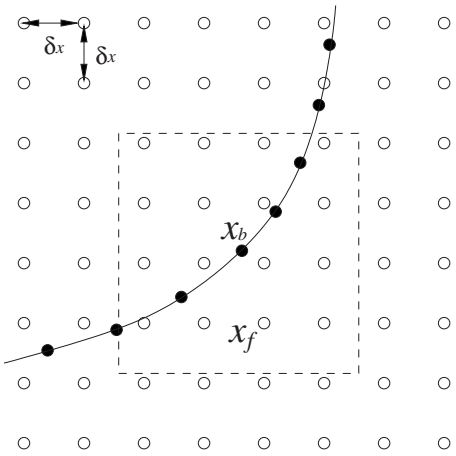

FIG. 1. A schematic of the immersed boundary method. The open circles are fluid nodes and the filled circles represent boundary nodes. The boundary force calculated at node $\mathbf{x}_b$ is distributed to the fluid nodes $\mathbf{x}_f$ in the $2d\times 2d$ square (dashed lines) through Eq. (7); and the velocity at $\mathbf{x}_b$ is obtained by interpolation from velocities at $\mathbf{x}_f$ through Eq. (10).

B. Immersed boundary method

Figure 1 displays a segment of boundary and the nearby fluid domain, where filled circles represent boundary nodes and open circles represent fluid nodes. In IBM, the boundary force $\mathbf{G}(\mathbf{x}_b)$ at a boundary marker $\mathbf{x}_b$, either physically induced by membrane deformation or artificially applied to generate a desired solid boundary velocity, is distributed to the nearby fluid grid points $\mathbf{x}_f$,

$$\mathbf{g}(\mathbf{x}_f)=\sum_b D(\mathbf{x}_f-\mathbf{x}_b)\mathbf{G}(\mathbf{x}_b), \tag{7}$$

through a discrete δ function $D(\mathbf{x})$, which is chosen to approximate the properties of the Dirac δ function [1,3,5]. In a two-dimensional system, $D(\mathbf{x})$ is given as

$$D(\mathbf{x}) = \frac{1}{4d^2}\left(1+\cos\frac{\pi x}{d}\right)\left(1+\cos\frac{\pi y}{d}\right),$$

$$|x| \leq d \quad \text{and } |y| \leq d, \tag{8}$$

$$D(\mathbf{x}) = 0 \quad \text{otherwise}. \tag{9}$$

Here d is one-half of the IBL thickness. In typical IBM simulations [1,3,5,6,10], $d=2\delta_x$. The boundary velocity $\mathbf{U}(\mathbf{x}_b)$ can be obtained in a similar way according to the local flow field,

$$\mathbf{U}(\mathbf{x}_b) = \sum_f D(\mathbf{x}_f - \mathbf{x}_b)\mathbf{u}(\mathbf{x}_f). \tag{10}$$

We point out that both the force distribution Eq. (7) and velocity interpolation Eq. (10) should be carried out in a $2d\times 2d$ region (dashed square in Fig. 1) [1,30], instead of a circular region of radius d as described elsewhere [3,31,32]. This is due to the specific approximation of the δ function Eq. (8) adopted in IBM. It can be shown that the sum of nonzero values of Eq. (8) in the square region is 1, and hence missing any nodes inside the square and outside of the circle of radius d would produce an inaccuracy in fluid forces and boundary velocity.

C. Immersed boundary lattice Boltzmann model for moving solid surfaces

In this work we employ the IB-LBM model proposed by Dupuis *et al.* [29] for its simplicity. At a certain time step t, according to the Navier-Stokes equation (5), if there is no force applied, the resulting velocity $\mathbf{u}^*$ at the next time step is given by

$$\frac{\mathbf{u}^*(\mathbf{x}_f, t+\delta_t) - \mathbf{u}(\mathbf{x}_f, t)}{\delta_t} = -(\mathbf{u}\cdot\nabla)\mathbf{u} - \frac{1}{\rho}\nabla p + \nu\nabla^2\mathbf{u}. \tag{11}$$

Including a body force $\mathbf{g}(\mathbf{x}_f, t)$ produces a different fluid velocity $\mathbf{u}$,

$$\frac{\mathbf{u}(\mathbf{x}_f, t+\delta_t) - \mathbf{u}_f(\mathbf{x}, t)}{\delta_t} = -(\mathbf{u}\cdot\nabla)\mathbf{u} - \frac{1}{\rho}\nabla p + \nu\nabla^2\mathbf{u} + \mathbf{g}(\mathbf{x}_f, t). \tag{12}$$

Therefore, to achieve a desired boundary velocity $\mathbf{U}^d$, the boundary force $\mathbf{G}$ should be related to velocities $\mathbf{U}^d$ and $\mathbf{U}^*$ as follows;

$$\mathbf{G}(\mathbf{x}_b, t) = \frac{\mathbf{U}^d(\mathbf{x}_b, t+\delta_t) - \mathbf{U}^*(\mathbf{x}_b, t+\delta_t)}{\delta_t}. \tag{13}$$

In IB-LBM simulations, the boundary force $\mathbf{G}$ in the above equation is calculated at boundary nodes, with $\mathbf{U}^*$ obtained from the corresponding values of neighboring fluid nodes through Eq. (10). Also the boundary force $\mathbf{G}$ is spread to these fluid nodes using Eq. (7).

III. SIMULATION EVIDENCE OF BOUNDARY SLIP

Our simulations are conducted over a 200×200 D2Q9 square lattice domain for three types of simple two-dimensional, steady, and incompressible flows, of which theoretical solutions are available.

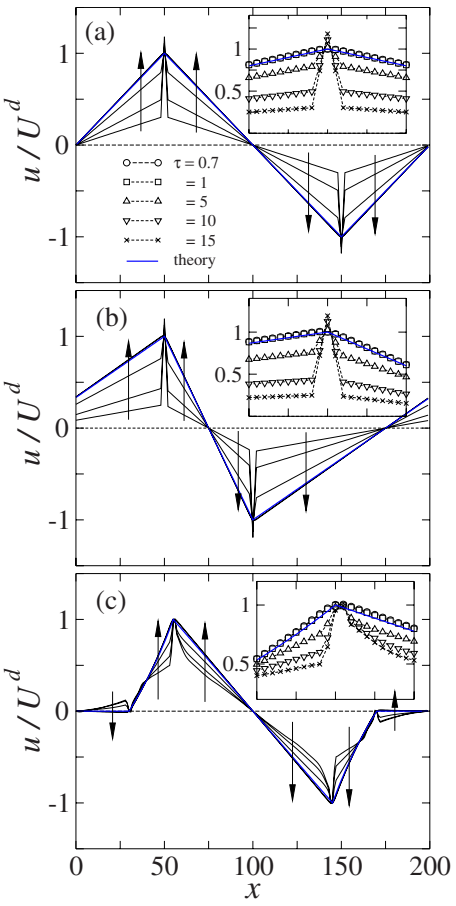

FIG. 2. (Color online) Profiles of the horizontal velocity at the vertical central plane $x=100\delta_x$ from IB-LBM simulations for (a) symmetric shear flows, (b) asymmetric shear flows, and (c) cylindrical Couette flows. The relaxation parameter τ changes from 15, 10, 5, 1, to 0.7 along the arrows. Also displayed in thick (blue) lines are the theoretical velocity profiles from fluid mechanics. The profiles in the peak regions are enlarged in insets.

(a) Symmetric shear flows: Two plain surfaces are placed at $y=50\delta_x$ and $y=150\delta_x$, and they are moving at opposite horizontal velocities, i.e., U^d and $-U^d$, respectively.

(b) Asymmetric shear flows: Same as the symmetric flows, except that the top plain surface is placed at $y=100\delta_x$.

(c) Cylindrical Couette flows: Two circular rings of radius of $45\delta_x$ and $70\delta_x$ are placed in the center of the simulation domain. The inner ring is rotating at U^d while the outer one is at rest.

For all these flow situations, general periodic boundary conditions are also applied in both x and y directions. Each plain surface or circular ring is represented by 800 evenly distributed boundary nodes. A wide range of the wall velocity U^d, from 10^{-7} to 10^{-1}, has been examined, and the results are identical, if only the simulation is stable.

Profiles of the velocity in x direction along the center vertical plain $x=100\delta_x$ with different relaxation parameter τ are plotted in Fig. 2. Here the velocities had been normalized with respect to the imposed boundary velocity U^d. According

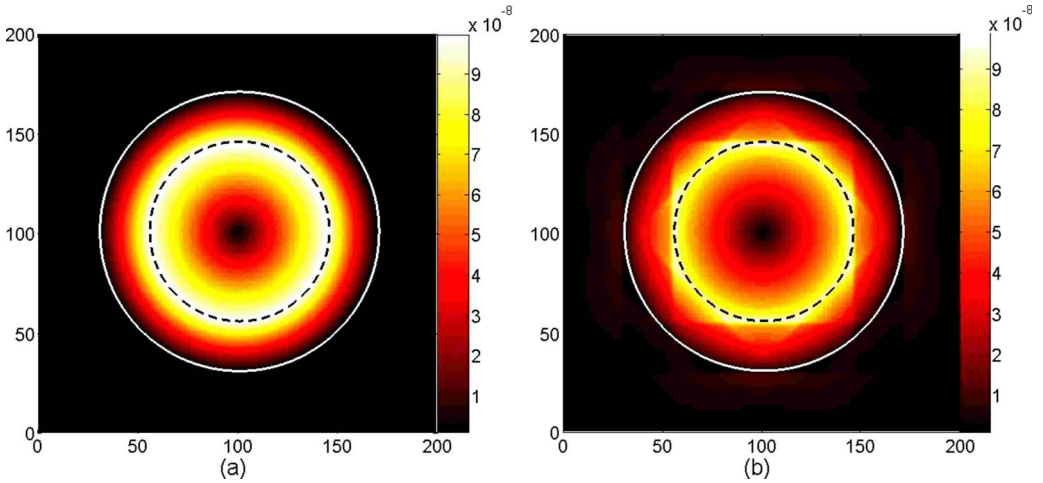

FIG. 3. (Color online) Tangential velocity of cylindrical Couette flows with (a) $\tau=1$ and (b) $\tau=10$. The dashed black and solid white circles indicate the positions of the rotating inner and stationary outer rings, respectively.

to basic fluid mechanics, the velocity distributions [thick (blue) lines in Fig. 2] in these simple flows are determined purely by their respective velocity boundary conditions, and independent to the fluid viscosity. However, this is obviously not true for the IB-LBM simulation results. The simulated results deviate from the theoretical predications greatly in all flow situations, especially at large τ values. For cases with small τ values ($\tau=0.7$ and 1), the IB-LBM profiles follow the theory better, but still not identical even with considering possible numerical errors. In general, a larger τ produces a smaller velocity gradient in the bulk region outside of the IBLs but a larger boundary velocity at the boundary position, when compared to the theoretical profiles. In spite of such discrepancy, the velocity profiles in bulk regions (i.e., linear profiles in shear flows and inside of the inner ring in cylindrical Couette flows, and $ar+b/r$ shape profiles between the two rings in cylindrical Couette flows; a and b are constants related to the ring rotating velocities and r is radius) can be well described by fluid mechanics, however, with different velocity boundary conditions as we imposed. This is not surprising since the general LBM algorithm can be mathematically considered as a Navier-Stokes solver. The difference between the simulated boundary velocity and that extrapolated from the bulk velocity profile according to fluid mechanics is usually called the boundary slip velocity [33–35]. It is worth to point out that the boundary slip observed here is purely a numerical artificial effect and it is different from the physical solid-liquid interfacial slip on hydrophobic surfaces [33–35]. In our simulation, the boundary slip velocity increases with the relaxation parameter τ.

Also it can be seen in Fig. 2 that the boundary velocity from IB-LBM does not satisfy the imposed boundary condition exactly, and the errors are large at high τ values. This has been noticed in previous studies [29] and is understandable by a careful examination of the IB-LBM scheme described in Sec. II C. The boundary force $\mathbf{G}$ is calculated from the could-be boundary velocity $\mathbf{U}^*$ without boundary force and the desired boundary velocity $\mathbf{U}^d$ through Eq. (13). This force is then distributed to its neighboring fluid nodes using Eq. (7). As a result, the velocity change at boundary, which is obtained by an interpolation of velocity differences at neighboring fluid nodes through Eq. (10), will not be the desired difference necessarily.

In addition, for the cylindrical Couette flows, we note that tangential velocity pattern is also affected by τ, which becomes not isotropic with a large τ value (Fig. 3). This could be due to the varying relative positions of boundary nodes to the underlying fluid Eulerian grid. Also, as suggested in previous studies of spurious currents in multiphase LBM models [36–38], the simple D2Q9 lattice structure may contribute to this nonisotropic pattern and more complicated lattice structures with higher degree of isotropy could be useful to reduce this effect.

IV. ANALYTIC SOLUTIONS OF THE SYMMETRIC FLOWS WITH IB-LBM

To have a better understanding of the above described τ effects on velocity fields in IB-LBM simulations, we perform a rigorous analysis of the density distributions and velocity in this IB-LBM model for symmetric shear flows by following a similar process proposed by He *et al.* [39]. For the simple two-dimensional, steady, and incompressible shear flow in x direction, we have

$$\rho = \text{const}, \quad v = 0, \quad \frac{\partial u}{\partial x} = 0, \quad \text{and} \quad \frac{\partial u}{\partial t} = 0. \tag{14}$$

According to Eqs. (1)–(3), at a steady state,

$$f_1^j = \frac{\rho}{9}\left(1 + \frac{3u_j}{c} + \frac{3u_j^2}{c^2}\right) + \frac{\delta_x \tau \rho G_j}{3c^2}, \tag{15}$$

$$f_3^j = \frac{\rho}{9}\left(1 - \frac{3u_j}{c} + \frac{3u_j^2}{c^2}\right) - \frac{\delta_x \tau \rho G_j}{3c^2}, \tag{16}$$

$$f_5^j = \frac{\rho}{36\tau}\left(1 + \frac{3u_{j-1}}{c} + \frac{3u_{j-1}^2}{c^2}\right) + \frac{\tau - 1}{\tau} f_5^{j-1} + \frac{\delta_x \rho G_{j-1}}{12c^2}, \tag{17}$$

$$f_6^j = \frac{\rho}{36\tau}\left(1 - \frac{3u_{j-1}}{c} + \frac{3u_{j-1}^2}{c^2}\right) + \frac{\tau-1}{\tau}f_6^{j-1} - \frac{\delta_x \rho G_{j-1}}{12c^2}, \tag{18}$$

$$f_7^j = \frac{\rho}{36\tau}\left(1 - \frac{3u_{j+1}}{c} + \frac{3u_{j+1}^2}{c^2}\right) + \frac{\tau-1}{\tau}f_7^{j+1} - \frac{\delta_x \rho G_{j+1}}{12c^2}, \tag{19}$$

$$f_8^j = \frac{\rho}{36\tau}\left(1 + \frac{3u_{j+1}}{c} + \frac{3u_{j+1}^2}{c^2}\right) + \frac{\tau-1}{\tau}f_8^{j+1} + \frac{\delta_x \rho G_{j+1}}{12c^2}. \tag{20}$$

Here the superscripts of density distribution f_i and subscripts of x velocity u and force G indicate the y position of the lattice node. The momentum density in the x direction is

$$\rho u_j = c[(f_1^j - f_3^j) + (f_5^j - f_6^j) + (f_8^j - f_7^j)]. \tag{21}$$

Using the Eqs. (15)–(20) and also considering the momentum change due to the applied force at a lattice node, it can be shown that

$$\rho u_j = \frac{\tau+1}{3\tau}\rho u_j + \frac{2\tau-1}{6\tau}\rho(u_{j-1} + u_{j+1}) + \frac{(5-4\tau)\delta_t \rho}{6}(G_{j-1} + G_{j+1} - 2G_j) + \frac{\delta_t}{\tau}\rho G_j. \tag{22}$$

Clearly, when the body force G_j is uniform, i.e., $G_j = G_0 = \text{const}$, the above expression reverts back to that in Ref. [39]. Simple algebraic manipulation of this equation yields

$$0 = \nu\frac{u_{j+1} + u_{j-1} - 2u_j}{\delta_x^2} + \frac{5\tau - 4\tau^2}{6}(G_{j-1} + G_{j+1} - 2G_j) + G_j, \tag{23}$$

which can be considered as a central finite different form of the simplified Navier-Stokes equation for our special case

$$0 = \nu\frac{\partial^2 u}{\partial y^2} + G(y). \tag{24}$$

Now starting from the moving plate at $y = j_0\delta_x$ ($j_0 = 50$ in our present simulations) and moving upward, we look at the velocity profile in such a symmetric shear flow. Due to the system symmetry, we have $u_{j_0+1} = u_{j_0-1}$. Also, according to the δ function given in Eq. (8), $G_{j_0} = G_0/2$, $G_{j_0\pm1} = G_0/4$, and $G_{|j-j_0|>1} = 0$, where G_0 is the total boundary force applied. Inserting these relations into Eq. (23) gives us the velocity differences between two adjacent lattice layers,

$$u_{j_0} - u_{j_0+1} = \frac{G_0\delta_x^2}{\nu}\left(\frac{1}{4} - \frac{5\tau - 4\tau^2}{24}\right), \tag{25}$$

$$u_{j_0+1} - u_{j_0+2} = \frac{G_0\delta_x^2}{\nu}\left(\frac{1}{2} - \frac{5\tau - 4\tau^2}{24}\right), \tag{26}$$

$$u_{j_0+2} - u_{j_0+3} = \frac{G_0\delta_x^2}{2\nu}. \tag{27}$$

Beyond the IBL, the force is 0 and the velocity gradient does not change anymore,

$$u_{j-1} - u_j = \frac{G_0\delta_x^2}{2\nu} \quad \text{for } j > j_0 + 2, \tag{28}$$

and the shear stress required to generate such a velocity gradient is

$$s = \mu\frac{\partial u}{\partial y} = \frac{1}{2}\rho G_0 \delta_x. \tag{29}$$

Therefore, the force needed to be applied at the moving plate per unit length δ_x is

$$F = 2s\delta_x = \rho G_0 \delta_x^2. \tag{30}$$

This equation shows that the hydrodynamics relationship between the applied force and the resulting bulk velocity gradient is always satisfied. However, in the boundary layers, the velocity gradients can be different from the bulk values dramatically, as we have seen from previous simulations. Combing Eqs. (25) and (26), we have

$$u_{j_0} = u_{j_0+2} + \frac{G_0\delta_x^2}{\nu}\left(\frac{3}{4} - \frac{5\tau - 4\tau^4}{12}\right), \tag{31}$$

whereas the theoretical prediction with a constant gradient given in Eq. (28) from the bulk region should be

$$\bar{u}_{j_0} = u_{j_0+2} + \frac{G_0\delta_x^2}{\nu}. \tag{32}$$

The difference between u_{j_0} and $\bar{u}_{j_0}$ is the artificial slip velocity from the IB-LBM model,

$$u_{j_0}^s = u_{j_0} - \bar{u}_{j_0} = \frac{4\tau^2 - 5\tau - 3}{12}\frac{G_0\delta_x^2}{\nu}. \tag{33}$$

The only τ value to make $u_{j_0}^s = 0$ is $\tau = (5+\sqrt{73})/8 \approx 1.693$, since another root of $u_{j_0}^s = 0$ is $\tau = (5-\sqrt{73})/8 < 0$ while the LBM algorithm requires $\tau > 1/2$. It can also be seen from this equation that the slip velocity will be more profound when τ becomes larger.

Since the velocity is zero at the center plane between the two shearing plates, and velocity gradients are known everywhere, we can easily find that

$$u_{j_0} = \frac{G_0\delta_x^2}{\nu}\left(\frac{h}{4} - \frac{1}{4} - \frac{5\tau - 4\tau^2}{12}\right) \tag{34}$$

and

$$u_{j_0\pm1} = \frac{G_0\delta_x^2}{\nu}\left(\frac{h}{4} - \frac{1}{2} - \frac{5\tau - 4\tau^2}{24}\right), \tag{35}$$

where h is the gap distance between the two moving plain surfaces ($h = 100$ in this work). Therefore, the boundary velocity calculated from u_{j_0} and $u_{j_0\pm1}$ with Eq. (10) is

$$U_b = \frac{G_0 \delta_x^2}{\nu}\left(\frac{h}{4} - \frac{3}{8} - \frac{5\tau - 4\tau^2}{16}\right). \tag{36}$$

We can also derive the relationship between the resulting boundary force G_0 and the imposed boundary velocity U_d using Eq. (13),

$$G_0 = \frac{U_d \nu}{\delta_x^2}\left(\frac{h}{4} - \frac{35}{72} - \frac{13\tau}{144} + \frac{\tau^2}{4}\right)^{-1}. \tag{37}$$

With these relations, we obtain the analytical expressions for the bulk velocity gradient du/dy, computed boundary velocity u_{j_0}, and boundary slip velocity $u_{j_0}^s$ as follows:

$$\frac{\left(\frac{du}{dy}\right)_{\text{bulk}}}{\frac{2U^d}{h\delta_x}} = \frac{\frac{h}{4}}{\frac{h}{4} - \frac{35}{72} - \frac{13\tau}{144} + \frac{\tau^2}{4}}, \tag{38}$$

$$\frac{u_{j_0}}{U^d} = \frac{\frac{h}{4} - \frac{1}{4} - \frac{5\tau}{12} + \frac{\tau^2}{3}}{\frac{h}{4} - \frac{35}{72} - \frac{13\tau}{144} + \frac{\tau^2}{4}}, \tag{39}$$

$$\frac{u_{j_0}^s}{U^d} = \frac{-\frac{1}{4} - \frac{5\tau}{12} + \frac{\tau^2}{3}}{\frac{h}{4} - \frac{35}{72} - \frac{13\tau}{144} + \frac{\tau^2}{4}}. \tag{40}$$

From fluid mechanics, we know that the velocity gradient in a shear flow is constant, $du/dy = 2U^d/h\delta_x$. Also with the no-slip boundary condition applied, the fluid velocity at boundary should be the same as the surface velocity imposed and therefore there is no slip between the solid and the adjacent fluid. Unfortunately, according to Eqs. (38)–(40), this can only be approximated if only h is large (a small lattice unit) and τ is small. This can be better seen in Fig. 4, where the fluid mechanics predictions (dashed lines), the analytical solutions derived above (solid lines), and the IB-LBM simulation results measured from Fig. 2(a) are plotted together. An excellent agreement can be found between our analytical solutions and computational simulations, proving the correctness of both our mathematical derivation and numerical implementation of IB-LBM. For the system studies here, Fig. 4 suggests that, to have a reasonable accuracy of IB-LBM simulation, the relaxation parameter τ should not be larger than 2.

V. EFFECT OF THE IMMERSED BOUNDARY LAYER THICKNESS

Another possible remedy to improve the velocity profiles from IB-LBM could be to increase the thickness of IBL, which has not been incorporated in the above analysis and simulations. To address this point, we change d (one-half IBL thickness) from $2\delta_x$, a typical choice in IBM studies [1,3,5,6,10], to $10\delta_x$ for symmetric shear flows with constant

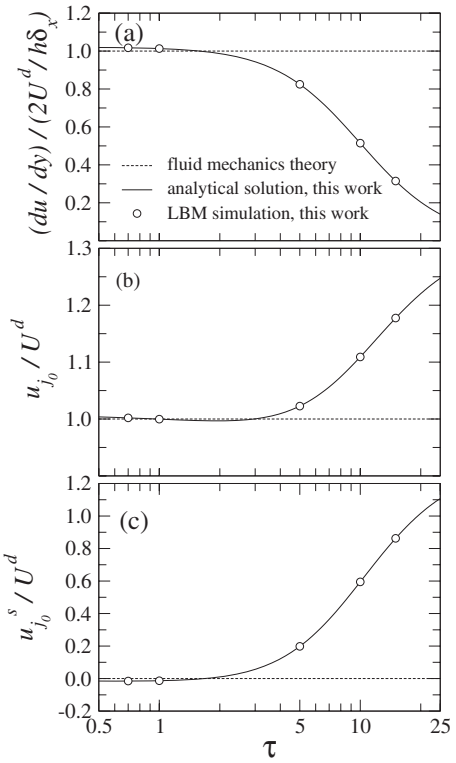

FIG. 4. (a) Bulk velocity gradient, (b) fluid velocity at boundary, and (c) boundary slip velocity from IB-LBM changing with the relaxation parameter τ.

$\tau = 10$. The simulated velocity profiles are displayed in Fig. 5. We can see that, as the IBL thickness increases, the velocity profile indeed approaches the theoretical solution [thick (blue) line]. However, such improvement is limited. Even with $d = 10\delta_x$, which means the IBL is $20\delta_x$ thick, the difference between simulation and theory is still very noticeable. Actually, the computational cost increases quickly with d,

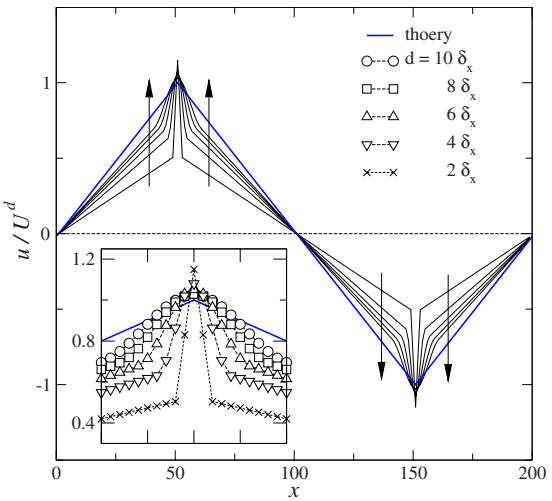

FIG. 5. (Color online) Velocity distributions of symmetric shear flows with $\tau = 10$ and one-half IBL thickness d changing from $2\delta_x$, $4\delta_x$, $6\delta_x$, $8\delta_x$, to $10\delta_x$ along the arrow directions. Also displayed as a thick (blue) line is the linear velocity distribution from fluid mechanics. The profiles in the peak regions are enlarged in the inset.

since a wider IBL implies more fluid nodes are involved in both the velocity interpolation and force distribution processes in IBM. Moreover, a thick IBL may prevent the applications of IBM to some certain systems, for example, of particulate suspensions [26], flexible filaments [40], and concentrated biofluids [24,25], where the particle size, membrane thickness, and gap between suspended particles or cells are small.

VI. SUMMARY AND CONCLUSIONS

IB-LBM simulations of simple plainer and cylindrical Couette flows have been conducted and the calculated velocity fields have been compared to theory. According to fluid mechanics, the velocity profiles of such flows are only determined by the imposed boundary velocity and are independent of the fluid properties such as density and viscosity. However, our simulations reveal severe deviation from theoretical predictions, especially at high relaxation parameter τ (or, equivalently, the kinematic viscosity ν) values. To have a better understanding of this important phenomenon, a rigorous analysis of the velocity from the IB-LBM algorithm has been carried out for a symmetric shear flow. The resulting solutions of fluid boundary velocity, bulk velocity gradient, and boundary slip velocity indicate their dependence on, in addition to the imposed boundary velocity, the relaxation parameter τ and gap distance between the two shearing plains. A good approximation to theory can only be achieved when both the lattice unit and δ_x and τ are small. The analytical solutions obtained for symmetric shear flows can also be useful for selecting a suitable relaxation parameter τ for other flow situations. For example, as demonstrated in Fig. 3, the tangential velocity distribution with $\tau=1$ is much better than that with $\tau=10$, in terms of both the pattern isotropy and boundary velocity agreement. For the system studied, the τ value should be less than 2 in order to have a reasonable accuracy from IB-LBM simulations.

The effect of IBL thickness has also been investigated numerically. Results show that a wider IBL can improve the discrepancy between computed and theoretical velocity profiles; however, such improvement is limited, and a good agreement cannot be achieved even with a 20-lattice unit wide IBL. Moreover, thick IBLs also require large computational resources, both in time and memory, and are not applicable to situations such as suspensions and filaments in flows.

Although the simulations and analysis in this paper are performed with a specific IB-LBM model, the results are qualitatively valid for other IB-LBM models. The only different point among the existing several IB-LBM models is their different methods in calculating the boundary force from the current velocity field and the desired boundary velocity. If only the boundary force is the same, the resulting velocity profiles from different IB-LBM models will be also the same, and the large deviation from theoretical predictions will always be there at high τ values. Although τ usually is small ($\tau<2$) in LBGK simulations; in certain circumstances, a wide range of τ may be necessary. For example, when simulating gas flows in microchannels, large τ values have been adopted to achieve high Knudsen numbers [41–44]. The aim of this paper is to address attentions of this interesting and important issue for meaningful IB-LBM simulations. As for any numerical methods, IB-LBM has its own strengths and weaknesses. Before we can remove or improve such weaknesses, it would be better for us to be aware of both of them and try our best to avoid the weaknesses.

ACKNOWLEDGMENTS

J.Z. acknowledges the financial support from the Natural Science and Engineering Research Council of Canada (NSERC) and a start-up grant from the Laurentian University. This work was made possible by the facilities of the Shared Hierarchical Academic Research Computing Network.

[1] C. S. Peskin, J. Comput. Phys. **25**, 220 (1977).
[2] G. Agresar, J. J. Linderman, G. Tryggvason, and K. G. Powell, J. Comput. Phys. **143**, 346 (1998).
[3] N. A. N'Dri, W. Shyy, and R. Tran-Son-Tay, Biophys. J. **85**, 2273 (2003).
[4] G. Tryggvason, B. Bunner, A. Esmaeeli, D. Juric, N. Al-Rawahi, W. Tauber, J. Han, S. Nas, and Y.-J. Jan, J. Comput. Phys. **169**, 708 (2001).
[5] C. D. Eggleton and A. S. Popel, Phys. Fluids **10**, 1834 (1998).
[6] P. Bagchi, P. C. Johnson, and A. S. Popel, J. Biomech. Eng. **127**, 1070 (2005).
[7] R. Dillon, L. Fauci, A. Fogelson, and D. Gaver III, J. Comput. Phys. **129**, 57 (1996).
[8] J. Mohd-Yusof, Annual Research Briefs, Center for Turbulence Research, 1997, pp. 317–327.
[9] E. A. Fedlun, R. Verzicco, P. Orlandi, and J. Mohd-Yusof, J. Comput. Phys. **161**, 35 (2000).
[10] R. Mittal and G. Iaccarino, Annu. Rev. Fluid Mech. **37**, 239 (2005).
[11] C. S. Peskin, Acta Numerica **11**, 479 (2002).
[12] S. Chen and G. D. Doolen, Annu. Rev. Fluid Mech. **30**, 329 (1998).
[13] R. Benzi, S. Succi, and M. Vergassola, Phys. Rep. **222**, 145 (1992).
[14] S. Succi, *The Lattice Boltzmann Equation* (Oxford University Press, Oxford, 2001).
[15] Y. Qian, D. DHumieres, and P. Lallemand, Europhys. Lett. **17**, 479 (1992).
[16] J. Zhang, B. Li, and D. Y. Kwok, Phys. Rev. E **69**, 032602 (2004).
[17] X. Shan and H. Chen, Phys. Rev. E **47**, 1815 (1993).
[18] J. Psihogios, M. E. Kainourgiakis, A. G. Yiotis, A. T. Papaioannou, and A. K. Stubos, Transp. Porous Media **70**, 279 (2007).

[19] J. Zhang and D. Y. Kwok, Langmuir **22**, 4998 (2006).
[20] J. Zhang and D. Y. Kwok, J. Colloid Interface Sci. **282**, 434 (2005).
[21] Y. Zhao, L. Wang, F. Qiu, A. Kaufman, and K. Mueller, Comput. Graph. **30**, 519 (2006).
[22] J. Zhang and D. Y. Kwok, J. Comput. Phys. **206**, 150 (2005).
[23] X. Fu, B. Li, J. Zhang, F. Tian, and D. Y. Kwok, Int. J. Mod. Phys. C **18**, 693 (2007).
[24] J. Zhang, P. C. Johnson, and A. S. Popel, J. Biomech. **41**, 4755 (2008).
[25] J. Zhang, P. C. Johnson, and A. S. Popel, Phys. Biol. **4**, 285295 (2007).
[26] Z. G. Feng and E. E. Michaelides, J. Comput. Phys. **195**, 602 (2004).
[27] X. Niu, C. Shu, Y. Chew, and Y. Peng, Phys. Lett. A **354**, 173 (2006).
[28] Y. Peng, C. Shu, Y. Chew, X. Niu, and X. Lu, J. Comput. Phys. **218**, 460 (2006).
[29] A. Dupuis, P. Chatelain, and P. Koumoutsakos, J. Comput. Phys. **227**, 4486 (2008).
[30] A. L. Fogelson and C. S. Peskin, J. Comput. Phys. **79**, 50 (1988).
[31] M. Francois, E. Uzgoren, J. Jackson, and W. Shyy, Int. J. Numer. Methods Heat Fluid Flow **14**, 98 (2003).
[32] H. S. Udaykumar, H.-C. Kan, W. Shyy, and R. Tran-Son-Tay, J. Comput. Phys. **137**, 366 (1997).
[33] D. C. Tretheway and C. D. Meinhart, Phys. Fluids **14**, L9 (2002).
[34] J. Zhang and D. Y. Kwok, Phys. Rev. E **70**, 056701 (2004).
[35] M. Cieplak, J. Koplik, and J. R. Banavar, Phys. Rev. Lett. **86**, 803 (2001).
[36] X. Shan, Phys. Rev. E **73**, 047701 (2006).
[37] M. Sbragaglia, R. Benzi, L. Biferale, S. Succi, K. Sugiyama, and F. Toschi, Phys. Rev. E **75**, 026702 (2007).
[38] J. Zhang and F. Tian, Europhys. Lett. **81**, 66005 (2008).
[39] X. He, Q. Zou, L. Luo, and M. Dembo, J. Stat. Phys. **87**, 115 (1997).
[40] L. Zhu and C. Peskin, Phys. Fluids **15**, 1954 (2003).
[41] H. Aminfar and M. Mohammadpourfard, J. Mech. Eng. Sci. **222**, 1855 (2008).
[42] C. Shen, D. Tian, C. Xie, and J. Fan, Microscale Thermophys. Eng. **8**, 423 (2004).
[43] X. Nie, G. Doolen, and S. Chen, J. Stat. Phys. **107**, 279 (2002).
[44] C. Lim, C. Shu, X. Niu, and X. Chew, Phys. Fluids **14**, 2299 (2002).